Chapter 2

LONG-TERM MEASUREMENTS OF RADON PROGENY CONCENTRATIONS WITH SOLID STATE NUCLEAR TRACK DETECTORS

K.N. Yu and D. Nikezic

Department of Physics and Materials Science, City University of Hong Kong,
Tat Chee Avenue, Kowloon, Hong Kong.

ABSTRACT

Inhaled radon (^{222}Rn) progeny are the most important source of irradiation of the human respiratory tract. Methods for long-term monitoring of the ^{222}Rn gas itself are well established, such as through the use of solid-state nuclear track detectors (SSNTDs). However, methods for long-term monitoring of the concentrations of radon progeny, or the equilibrium factor F, are still being actively explored. A brief review of existing methods for long-term measurements of radon progeny concentrations or F with SSNTDs will first be given.

In 2004, a method known as the proxy equilibrium factor (F_p) method was proposed to determine F using the bare LR 115 detector. F_p was equal to the ratio between the sum of concentrations of the two alpha emitting radon progeny (^{218}Po+^{214}Po) to the concentration of ^{222}Rn, was found to well correlate with F. The F_p method will be described in details in this chapter. Factors affecting the F_p method such as the removed active layer of the LR 115 detector during chemical etching, presence of ^{220}Rn in the ambient environment, and deposition of dust particles on the bare LR 115 detector are also discussed. Some applications of the F_p method are then presented, including long-term measurements of radon and thoron concentrations and F in dwellings, passive monitoring of F inside a radon exposure chamber, and derivation of V function for LR 115 SSNTDs.

1. INTRODUCTION

Inhaled radon (^{222}Rn) progeny are the most important source of irradiation of the human respiratory tract. Epidemiological studies of underground miners of uranium and other minerals have provided reasonably firm estimates of the risk of lung cancer associated with exposure to radon progeny (e.g., Lubin et al., 1995; Muirhead, 1997; NRC, 1999). It is well established that the absorbed radon dose in the lung is mainly due to radon progeny, but not the radon gas itself. Therefore, long-term measurements of the concentrations of radon progeny or the equilibrium factor F, together with a measurement or an estimation of the aerosol size distribution, are needed to accurately assess the health hazards contribution from radon progeny.

The equilibrium factor F of a given mixture of radon progeny in air is defined as the ratio $F = C_e/C_0$ where C_e is the radon gas concentration in equilibrium with its progeny which have the same potential alpha energy concentration as the given mixture of radon progeny and C_0 is the real radon concentration. F can also be calculated as

$$F_{^{222}Rn} = 0.105 f_{^{218}Po} + 0.515 f_{^{214}Pb} + 0.380 f_{^{214}Bi,Po} \tag{1}$$

where f_i is the ratio of the activity concentration the ith radon decay product to that of ^{222}Rn, i.e., $f_1 = f_{^{218}Po}$, $f_2 = f_{^{214}Pb}$ and $f_3 = f_4 = f_{^{214}Bi,^{214}Po}$.

Methods for long-term monitoring of the ^{222}Rn gas itself are well established, such as through the use of solid-state nuclear track detectors (SSNTDs) (see e.g., Nikolaev and Ilic (1999) for a survey). When alpha particles strike a SSNTD, latent tracks will be formed, which will become visible under the optical microscope on suitable chemical etching. In general practice nowadays, the radon gas concentration is first determined and an assumed F between radon and its progeny, typically from 0.4 to 0.5 is then applied. The exposure to radon progeny can be expressed in the traditional unit *working level month* (WLM) and then multiplied with the dose conversion coefficient (DCC) by assuming a given aerosol size distribution to give the effective dose. However, in reality, the concentrations of radon and its progeny vary significantly with time and place. Therefore, an assumed F cannot reflect the actual conditions. This problem cannot be solved through active measurements based on air filtering, since they only give short-term measurements. As a result, methods for long-term monitoring of the concentrations of radon progeny or F have been actively explored. A brief review of existing methods for long-term measurements of radon progeny concentrations or F with SSNTDs is given in section 2 below.

2. EXISTING METHODS FOR LONG-TERM MEASUREMENTS OF RADON PROGENY WITH SSNTDS

Amgarou et al. (2003), Nikezic and Yu (2004) and Yu et al. (2005) made surveys of previous methods for determining F and concluded that all those methods suffered from some problems. Here we will give some more detailed description of the methods and problems involved.

The first method was proposed by Frank and Benton (1977). In this method, cellulose nitrate detectors were used, one in a diffusion chamber and the other as an open detector. The open detector registered the total concentration of α-particle-emitting nuclei in air, i.e., ^{222}Rn + progeny (^{218}Po+^{214}Po), while the closed detector measured only ^{222}Rn. The ratio between the readings for the open and closed detectors was related to F and from there it should be possible to estimate F. The track density on the open bare detector ρ_{open} is given as $\rho_{open} = (\rho_0 C_0 + \rho_1 C_1 + \rho_3 C_3)t$, where C_0, C_1 and C_3 (=C_4) are concentrations of ^{222}Rn, ^{218}Po and ^{214}Bi(^{214}Po) in open air, respectively; ρ_0, ρ_1 and ρ_3 are partial sensitivities of bare detector to ^{222}Rn, ^{218}Po and ^{214}Bi(^{214}Po), respectively; and t is the exposure time. The partial sensitivities ρ_i of the bare detector to radon and its progeny are the numbers of tracks per unit area per unit exposure, i.e., they have the unit of (m^{-2})/(Bq m^{-3}s) or just (m)). The number of tracks on the closed detector (inside the diffusion chamber) is given as $\rho_{closed} = \rho_C C_0$, where ρ_C is the sensitivity of closed detector. The ratio between the track densities on the bare and the closed detectors is then given as

$$\frac{\rho_{open}}{\rho_{closed}} = \frac{\rho_0}{\rho_C} + \frac{\rho_1}{\rho_C}\frac{C_1}{C_0} + \frac{\rho_3}{\rho_C}\frac{C_3}{C_0} = \frac{\rho_0}{\rho_C} + \frac{\rho_1}{\rho_C}f_{^{218}Po} + \frac{\rho_3}{\rho_C}f_{^{214}Bi,Po}.$$ This ratio has some

resemblance with Eq. (1), but the term $f_{^{214}Pb}$ is missing here, and the coefficients for the terms $f_{^{218}Po}$ and $f_{^{214}Bi,Po}$ are also different. Furthermore, an additional term ρ_0 / ρ_C appears here. It is apparent that additional effort should be devoted to derive the equilibrium factor F from the ratio $\rho_{open} /\rho_{closed}$. Although this method was used by many authors under different detector setups, due to the differences mentioned above, it could not give realistic results. Another problem for this method was the assumption that the sensitivities for the open and closed detectors for each of the α-emitting radionuclide in the ^{222}Rn decay chain were the same. This assumption was not correct because the sensitivity of the closed detector depended on the chamber shape and dimensions as well as other construction details, and might be very different from the sensitivity of an open detector.

Another method was proposed by Fleischer (1984) who used four detectors for radon progeny measurements. Three detectors were covered with polyethylene absorber foils with different thickness. The bare detector and the first one with a 20 μm absorber could detect alpha particles emitted by ^{222}Rn and the progeny ^{218}Po+^{214}Po. Another two with thicker absorbers measured α emissions from ^{218}Po+^{214}Po and ^{214}Po. By this method, the α-active progeny (^{218}Po and ^{214}Po) could be measured separately. However, this method failed because of unavoidable progeny deposition (plate-out) on the detectors and on the absorber foils. The amount of deposition was not known, and might be variable. The deposited progeny had much larger detection probability and this effect significantly affected the progeny measurements.

A second group of methods was based on the assumption that F depended mainly on the ventilation rate. In fact, several processes affected the concentration ratio of progeny to radon, such as deposition and ventilation. The model of Jacobi (1972) described the balance of radon and its progeny in a closed space. If all other parameters were kept at their best estimates, from the ratio of the track density on the open and closed detectors, one could infer the ventilation rate and F (Planinic and Faj, 1990). However, this method failed for two reasons.

The first one was that F was a weak function on the ventilation rate. Actually, the radon concentration was very dependent on the ventilation rate, but the ratio of progeny concentrations to the radon concentration was not. The dependence of F on the ventilation rate is shown in Figure 1.

For nominal ventilation rates between 0.5 and 1.5 h^{-1}, F varies between 0.32 and 0.23 (if other parameters are kept constant). This change is relatively small, and if we take into account other uncertainties, such as statistical errors in the number of the tracks, etc., the determination of F through measurements of the ventilation rate becomes problematic. Another reason why this method failed was that the deposition rates of radon progeny could be very different from the "typical" values. Another deficiency of the method was the assumption on equal sensitivities of the open and closed detectors.

One extension of this method was proposed by Dorschel and Piesch (1993). In this method, special etching conditions had to be applied on the track detector so that the energy window was between 6.05 and 7.5 MeV. In this way, only ^{214}Po in air was measured. From the ratio $f_{^{214}Po}$ of concentrations between ^{214}Po and ^{222}Rn, one could obtain F. This method was also based on the assumption that all other parameters were kept at their best estimations except the ventilation rate. The method was better than the previous one, because F was better correlated to $f_{^{214}Po}$ than to the track density ratio between the open and closed detectors, but there were difficulties to realize such a narrow energy window. The calibration was also a problem because it was not easy to obtain air contaminated only with ^{214}Po whose concentration should be known. Here, the calibration factor had to be calculated.

Nikezic and Baixeras (1996) proposed the barrier method for which barriers were placed at some distances in front of LR 115 detectors. Due to the differences in the alpha energies emitted from different progeny and the existence of an upper limit in the energy window for the LR 115 detector, separation of progeny had been shown to be theoretically possible. An alpha particle had to travel some distance in the air before its energy fell below the upper limit in the energy window to be detected. If the barrier was too close, the LR 115 detector would not detect any alpha particle. If the barrier was a little bit farther away, it would detect alpha particles from radon only, and so on. However, experimental verification of this method was not successful because of plate-out of radon progeny on the barrier, for which the theoretical model failed to describe.

Another class of methods was based on spectrometry of alpha particles. From the track parameters, it was possible to determine the energy of alpha particles that produced the tracks. However, the track parameters were dependent on the incident angle in addition to the incident energy. Therefore, the same track parameters (major and minor axes) could be obtained with different incident energies. Other track parameters were needed, such as the average gray level or the track shape. Even the establishment of the incident alpha-particle spectrum from the track parameters was difficult by itself and tedious. The second step would be the interpretation of the data and linking the obtained spectra with F or to the concentration of particular radon progeny. The incident alpha-particle spectrum depended on the relative concentrations of radon progeny in air. In Figure 2, incident alpha-particle spectra are given, where $f(E)$ refers to the fraction of alpha particles incident on the open detector with an energy between E and $E+dE$ (Nikezic and Yu, 2002a).
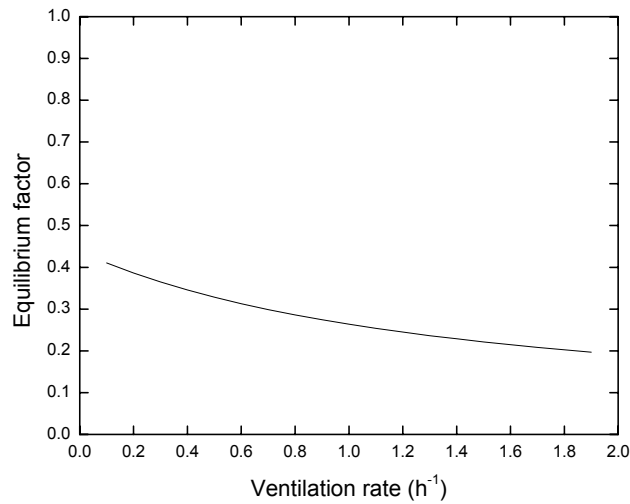
Figure 1. Equilibrium factor as a function of the ventilation rate. Other parameters: aerosol attachment rate $\lambda_a = 50$ h^{-1}, deposition rate of unattached progeny $\lambda_{d,u} = 20$ h^{-1} and deposition rate of attached progeny $\lambda_{d,a} = 0.2$ h^{-1}, recoil factor 0.83. (Adopted from Yu et al. 2005.)
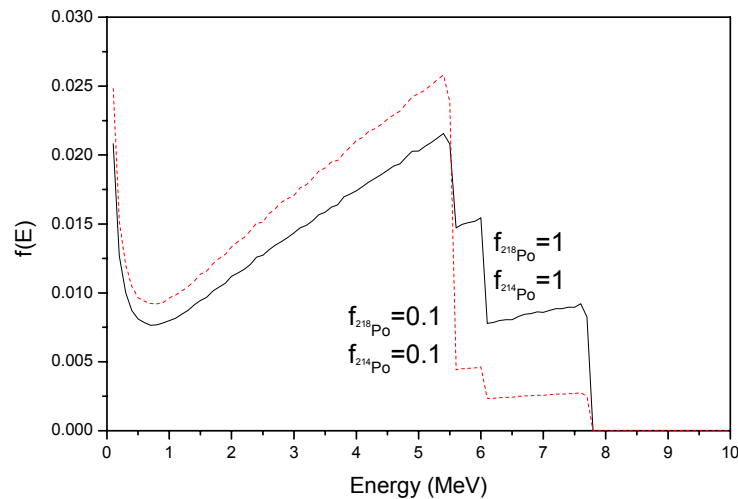

Figure 2. Incident alpha-particle spectra for two extreme ratios of progeny to radon concentrations (Nikezic and Yu, 2002a).

In Figure 2, the spectra for two extreme cases are given, namely, for an equilibrium factor $F = 1$ and for a low equilibrium factor $F = 0.1$. The curves in Figure 2 show a non-Gaussian peak at 5.49 MeV and cutoff structures above 5.49 MeV. The first cutoff from right to left is related to ^{214}Po while the second to ^{218}Po. The curves have plateaus between 6 and 7.69 MeV and between 5.49 and 6 MeV; the former (^{214}Po plateau) is wider because of the wider energy gap, while the latter (^{218}Po plateau) is narrower and higher than the ^{214}Po plateau. By analyzing the height of these two plateaus, one can infer some information about the relative activities of ^{218}Po and ^{214}Po. If their activities are equal (as shown in Figure 2, where $f_{^{218}Po} = f_{^{214}Po}$), the ^{218}Po plateau is two times higher than the ^{214}Po plateau.
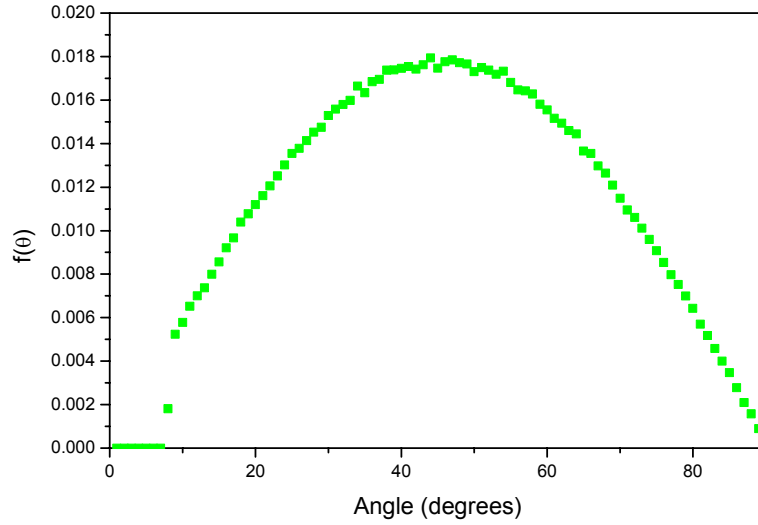
Figure 3. Angular distribution of incident alpha particles onto the detector (Nikezic and Yu, 2002a).

The process of plateout will create two intensive peaks at 6 and 7.69 MeV in the measured spectrum. The heights of these peaks depend on the amount of plateout as well as the efficiency and energy resolution of the detector and the measuring conditions. The most important part of the spectrum is between 6 and 7.69 MeV. Here, only [214]Po from air contributes to the detector response. In order to avoid the influence of plateout (if SSNTDs are considered), the energy window between 6.2 and 7.5 should be considered. Actually the width of the window depends on the energy resolution attainable in measurements, but of course, it should not be wider than the range from 6 to 7.69 MeV. If the energy resolution is worse than 1 MeV, measurements of radon progeny would not be possible by analyzing the energy spectrum. The feasibility of radon progeny measurement relies on the provision of high-resolution alpha spectroscopy.

One extension of the spectroscopy method was to measure only tracks with the ratio of major to minor axes in some ranges, so that only particles that enter the detector with an angle close to normal incidence were counted (Hadler and Paulo, 1994). In Figure 3, the angular distribution of incident alpha particles is given. From this figure, it is clear that a very small number of particles will hit the detector with an angle close to 90[o]. Therefore, the method mentioned above had to be very tedious since the number of tracks satisfying the given condition was rather small. Although the tediousness could be resolved by using automatic image analysis systems, the low sensitivity caused by the selection of the tracks remained an intrinsic limitation.

A more feasible method was proposed by Amgarou et al. (2003) who measured the equilibrium factor through the so-called "reduced" equilibrium factor, which was defined as

$$F_{\mathrm{Re}d} = 0.105 f_{^{218}Po} + 0.380 f_{^{214}Bi,Po} \tag{2}$$

Employment of three detectors was proposed in application of this method. The first one was closed inside a diffusion chamber, which measured radon only. Two open detectors were used with different energy windows for separate measurements of [218]Po and [214]Po. The

etching conditions applied to the Makrofol detectors for the required energy window were also determined. The reduced equilibrium factor F_{Red} was then calculated. It was further shown that F depended on F_{Red} in a very good manner, as shown in Figure 4. Comparisons with experimental data obtained from direct active measurements have shown very good agreement (Amgarou et al. 2003).

More recently, Nikezic et al. (2004) proposed measurements of F through the so-called "proxy equilibrium factor" F_p, which was a feasible method for long-term measurements of F. The method will be introduced in more details in section 3 below.

3. PROXY-EQUILIBRIUM FACTOR (F_P) METHOD

Nikezic et al. (2004) and Yu et al. (2005) proposed to use the bare LR 115 detector (12 μm red cellulose nitrate on a 100 μm clear polyester base, from DOSIRAD, Type 2, Non Strippable), which is a commonly used SSNTD, for determining the airborne ^{218}Po+^{214}Po concentration, and show that this concentration can be employed to give good estimates of F for the radon progeny in an environment. The LR 115 detector has an upper energy threshold for track formation, which is well below the energy of alpha particles emitted by the radon progeny plate out on the detector, i.e., plate-out progeny are not detected by LR 115.

3.1. Determination of Response of LR 115

In this section, the response of the bare LR 115 detector to ^{222}Rn and its alpha emitting short-lived progeny, i.e., ^{218}Po and ^{214}Po will be determined. The task is to study the response in terms of partial sensitivities ρ_i of the detector to radon and its progeny (i.e., the number of tracks per unit area per unit exposure, i.e., the unit of (m^{-2})/(Bq m^{-3}s) or just (m)).
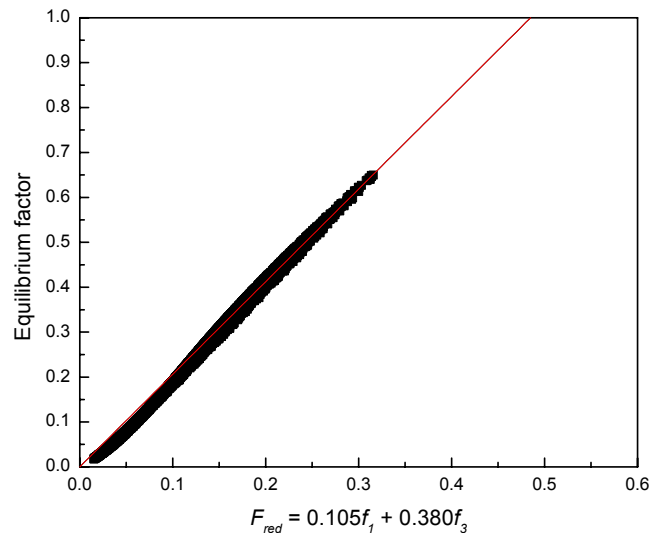

$$F_{red} = 0.105f_1 + 0.380f_3$$

Figure 4. The ^{222}Rn progeny equilibrium factor expressed as a function of the reduced equilibrium factor, calculated for all possible values for the parameters in the Jacobi model.

The Monte Carlo method was employed by Nikezic et al. (2004) and Yu et al. (2005) to determine the detector responses. To apply this method, a sampling volume had to be defined. A cross section of such a sampling volume is shown in Figure 5. The initial points of alpha particles in the simulations have been chosen in such a way that their distances to the detector are less than the range R of the alpha particles in air. They are also chosen so that the incident angle to the detector is larger than the theoretical critical angle θ_{lim}, which is defined as $\theta_{lim} =$ $\sin^{-1}(1/V_{max})$ where V_{max} is maximal value of the V function (the ratio of the track etch rate V_t to the bulk etch rate V_b, i.e., $V = V_t/V_b$). Particles striking the detector with an angle smaller than θ_{lim} cannot produce any track.

To determine the incident energy of an alpha particle when it strikes the detector, the SRIM program (http://www.srim.org/) is employed. The stopping-power data are used to produce energy-distance tables for alpha particles in air; these are graphically presented in Figure 6. The energy E_x of the alpha particle incident on the detector after traveling a distance in air is determined by linear interpolation between data in the corresponding energy–distance table. The ranges of alpha particles in the LR 115 detector (cellulose nitrate) are also determined using the data obtained from the SRIM program.
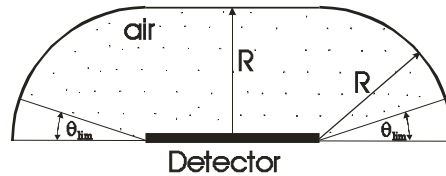

Figure 5. Cross section of the sampling volume of initial points of alpha particles in the simulation. R is range of alpha particles in air, while $\theta_{lim} = \sin^{-1}(1/V_{max})$ is critical angle. The 3-D object is obtained by rotation of the curve around the normal onto the detector. (Adopted from Yu et al. 2005.)
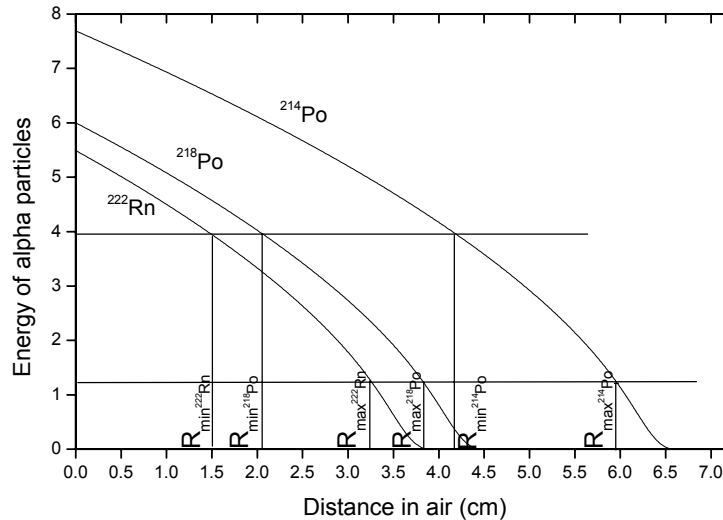

Figure 6. Energy–distance curves for radon and its progeny in air. The alpha particles emitted from a distance between R_{min} and R_{max} will strike the detector with an energy within the energy window for LR 115 between 1.25 and 3.9 MeV. In all cases, $R_{max} - R_{min} \approx 1.7$ cm (see Table 1).

Table 1. The values of R_{min} and R_{max} calculated for energies of alpha particles in the radon chain using data for stopping power given by the SRIM program.

Alpha energy (MeV)	Range (cm)	R_{min} (cm)	R_{max} (cm)	$R_{max} - R_{min}$ (cm)
5.49	3.85	1.5	3.25	1.75
6.00	4.42	2.1	3.82	1.72
7.69	6.55	4.2	5.95	1.75

Yu et al. (2005) determined the distributions of lengths of major and minor axes of alpha-particle tracks in the LR 115 detector produced by [222]Rn, [218]Po and [214]Po. The Monte Carlo program developed by Nikezic and Yu (1999) was employed. The lengths of major and minor axes were calculated by the model developed by Nikezic and Yu (2003).

The partial sensitivities depend on the V function ($V = V_t/V_b$) as well as the thickness of the removed active layer during etching. Yu et al. (2005) tried to illustrate the concept behind their proposed method and adopted the V function published by Durrani and Green (1984) in their preliminary calculations. The use of different V functions, however, will not affect the conclusions.

Yu et al. (2005) also used a removed active layer (i.e., the removed cellulose nitrate layer) of 6.54 μm as an example [taking $V_b = 3.27$ μm h^{-1} (Nikezic and Janicijevic 2002) and etching for 2 h]. The initial thickness of LR 115 was taken as 12 μm as declared by the manufacturer, so the residual thickness of the active layer was 5.46 μm. The bulk etch rate of the LR 115 detector was indirectly determined by many authors in the past (Somogyi and Hunyadi, 1978; Nakahara et al., 1980) through measurements of track radii after irradiation to fission fragments. Direct measurements of V_b were made by Nikezic and Janicijevic (2002) and Yip et al. (2003a). It is also noted that the actual removed active layer varies from sample to sample, and stirring significantly enhances the bulk etch rate (Yip et al., 2003a).

In the course of simulations, only the tracks which perforate the active layer of the LR 115 detector are considered. During actual counting, completely perforated tracks are easier to identify due to the different colors at the bottom of the track when compared to the non-perforated tracks. This visibility criterion is introduced in order to minimize the level of subjectivity. All the tracks were selected according to the lengths of their major and minor axes, with steps of 0.2 μm. When the calculations were completed, the number distribution N_j is obtained, which is the number of tracks within a unit detector area with the length of the major axis between D_j and $D_j + 0.2$ μm. The number distribution is then divided by the total number of the tracks to give the probability distribution p_j, which represents the probability of a particle creating a track with the major axis length between D_j and $D_j + 0.2$ μm. The ratio $p_j/0.2$ is the probability density δ_j (in m^{-1}).

The next step was the multiplication of δ_j with εVCt, where V is the volume (m^3) of the space where the initial points of alpha particles were chosen (Figure 5), C (Bq/m^3) the concentration of alpha emitters (radon or radon progeny in our case) in air, ε the detection efficiency expressed as the ratio between the number of particles creating perforated tracks in the detector to the total number of emitted particles, and t (s) is the time of irradiation. Since VCt is the number of alpha particles emitted in the time interval t in the space above the detector, εVCt is the number of the tracks created in a unit area of the detector. Therefore, the product $\delta_j \varepsilon VCt$ is the number distribution for the given exposure Ct, i.e., the probability to

obtain a track with the major axis in the range (D, $D + dD$) for the exposure Ct. We denote this product $\delta_j \varepsilon VCt$ as (dN/dD) where N is the number of tracks for a unit detector area. If we assume that $Ct = 1$ Bq.s.m^{-3}, (dN/dD) for a unit exposure and a unit detector area is obtained. The same formulations will apply for the cases of the minor axis.
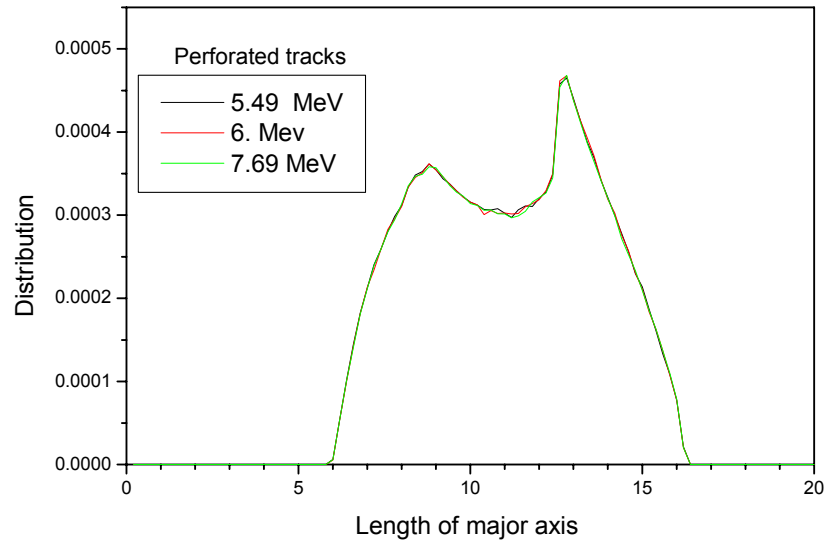
3.2. Theoretical Results and Discussion

Figure 7. Distribution (see text for definition) of the length of major axes for perforated tracks in LR 115. (Adopted from Yu et al. 2005.)
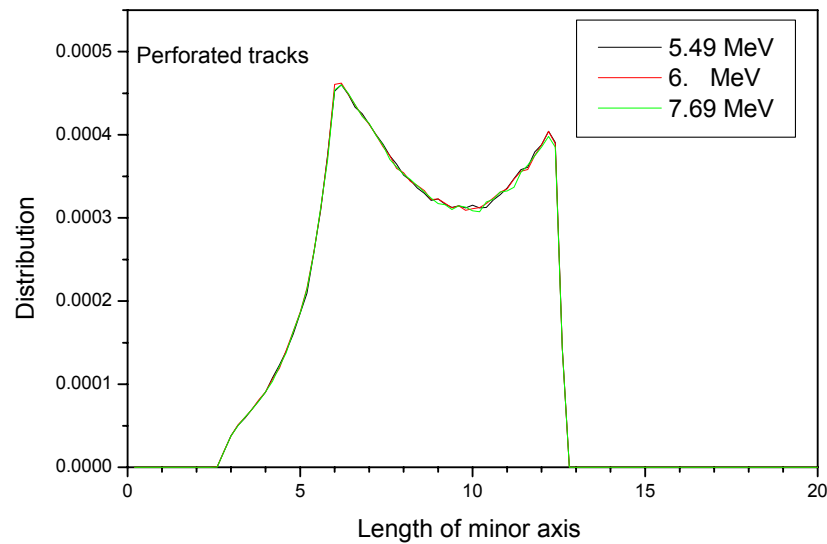

Figure 8. Distribution (see text for definition) of the length of minor axes for perforated tracks in LR 115. (Adopted from Yu et al. 2005.)

Figures 7 and 8 show the distribution (dN/dD) of the major and minor axes of perforated tracks in the LR 115 detector, respectively, for a unit exposure and a unit detector area ($dN = \delta_j \varepsilon V C t \, dD = \delta_j \varepsilon V \, dD$ for a unit exposure). From Figure 7, the lengths of the major axes are between 6 and 16 μm with two maximums, the more pronounced one being at about 13 μm (longer tracks), and the less pronounced one being at about 9 μm (shorter tracks). From Figure 8, the lengths of the minor axes are between 2.5 and 13 μm also with two maximums, the more pronounced one being at about 6 μm (narrower tracks), and the less pronounced one being at about 12 μm (wider tracks). The bimodal distributions can be explained through analyses of angular and energy distribution of alpha particles incident on the detector and are related to the track formation model. The peaks corresponding to longer axes are created by alpha particles with incident energies between 1.5 and 2.5 MeV, while the peaks corresponding to shorter axes originated from alpha particles with incident energies between 3 and 4 MeV.

3.3. Equality of Partial Sensitivities

It is interesting to observe from Figures 7 and 8 that the curves (dN/dD)$_i$ for three alpha energies i in the radon chain overlap completely for the entire ranges of the length for both major and minor axes. From this result, we see that $\rho_i = \int (dN/dD)_i \, dD$ are the same for different i, where ρ_i is the number of tracks on a unit detector area for a unit exposure to the alpha energy i in the radon chain, or in short, the partial sensitivity for i. In other words, *the partial sensitivities ρ_i of the LR 115 detector to ^{222}Rn, ^{218}Po and ^{214}Po are the same.* It is remarked here that the equality of partial sensitivities arises because of the presence of the upper energy threshold for recording alpha-particle tracks in LR 115. For other detectors without the upper energy threshold, e.g., CR-39, the partial sensitivities will not be the same.

A simplified explanation for the equality of partial sensitivities of the LR 115 detector to ^{222}Rn, ^{218}Po and ^{214}Po is given as follows (neglecting some minor details such as the critical angle for track formation). The probability P of an alpha particle emitted at the point $A(r,\theta,\varphi)$ hitting a point-like detector at the origin of the coordinate system with a surface area S is given as $S \cos\theta/(4\pi r^2)$, so the average detection efficiency is proportional to:

$$\int P dV = \iiint \frac{S \cos\theta}{4\pi r^2} r^2 \, dr \sin\theta \, d\theta \, d\varphi \propto \int_{R_{min}}^{R_{max}} dr \propto (R_{max} - R_{min}) \qquad (3)$$

where R_{min} and R_{max} are the minimum and maximum distances, respectively, of the alpha emitters from which the alpha-particle energies will fall within the energy window of the LR 115 detector. It is apparent that the ($R_{max} - R_{min}$) values are the same for ^{222}Rn, ^{218}Po and ^{214}Po, since the ($R_{max} - R_{min}$) value is in fact controlled by the energy window of the LR 115 detector. Therefore, $\rho_i = \rho_{^{222}Rn} = \rho_{^{218}Po} = \rho_{^{214}Po}$. It is remarked here that the equality of partial sensitivities arises because of the presence of the upper energy threshold for recording alpha-particle tracks in LR 115, so the lower limit of integration in Eq. (3) is R_{min}. For other detectors without the upper energy threshold, e.g., CR-39, the lower limit of integration in Eq.

(3) becomes 0, so $\int P dV$ will be proportional to R_{max} instead of $(R_{max} - R_{min})$, and the partial sensitivities will not be the same. The difference $(R_{max} - R_{min})$ does not depend on the alpha-particle emitter because the energy-distance curves are parallel to one another for different emitted alpha-particle energies (see Nikezic et al. 2004), while R_{max} depends on the alpha-particle emitter. One should also note that the energy window of the LR 115 detector depends on the removed active layer upon chemical etching. With prolonged etching, the energy window becomes wider, i.e., the upper energy threshold becomes higher in energy, and the lower energy threshold becomes lower in energy. If the energy window is too large, which is obtained for very large removed layers, the upper energy threshold might become larger than 5.49 MeV which is the energy of alpha particles emitted by ^{222}Rn. In this case, the equality of partial sensitivities is impaired.

3.4. Equilibrium Factor Determination

Knowing that the partial sensitivities are equal, the total track density ρ (in track/m^2) on the detector is $\rho = \rho_i (C_0 + C_1 + C_3) \cdot t$, where C_0, C_1 and C_3 are the concentrations ^{222}Rn, ^{218}Po and ^{214}Bi(Po) in Bq/m^3 and t is the exposure time in s. The proxy-equilibrium factor F_p was defined as (Nikezic et al., 2004 and Yu et al., 2005)

$$F_p = f_1 + f_3 = \frac{C_1}{C_0} + \frac{C_3}{C_0} = \frac{\rho}{\rho_i \cdot t \cdot C_0} - 1 \tag{4}$$

To determine the equilibrium factor F from the proxy-equilibrium factor F_p, a method similar to that devised by Amgarou et al. (2003) to determine F from the reduced equilibrium factor F_{red} is employed. Amgarou et al. (2003) calculated equilibrium factors through the Jacobi (1972) room model by systematically varying all parameters that influence the concentrations of radon and its progeny, and plotted them with F_{red}. The procedures are repeated, but with F_{red} replaced by F_p, and the results were given by Yu et al. (2005) and reproduced here in Figure 9 (which is in fact equivalent to Figure 1 of Amgarou et al. (2003) with a shift of one unit). It is observed that F_p has a good correlation with F so the F_p method is a convenient method for the determination of F with the LR 115 detector.

The method proposed by Amgarou et al. (2003) through F_{red} involved measurements of ^{218}Po and ^{214}Po concentrations. These relied on particular etching conditions on the Makrofol detector to enable the counting of alpha tracks in two energy windows, viz., (3 – 5 MeV) for ^{222}Rn and ^{218}Po, and (6.3 – 7.5 MeV) for ^{214}Po. The determination of F from F_p is simpler and more convenient.

In section 4 below, we will further look into the details for F_p and study the potential factors affecting the measurements of F using this technique. These factors include (1) the removed active layer of the LR 115 detector, (2) the presence of ^{220}Rn in the ambient environment, and (3) the deposition of dust particles on the LR 115 detector.
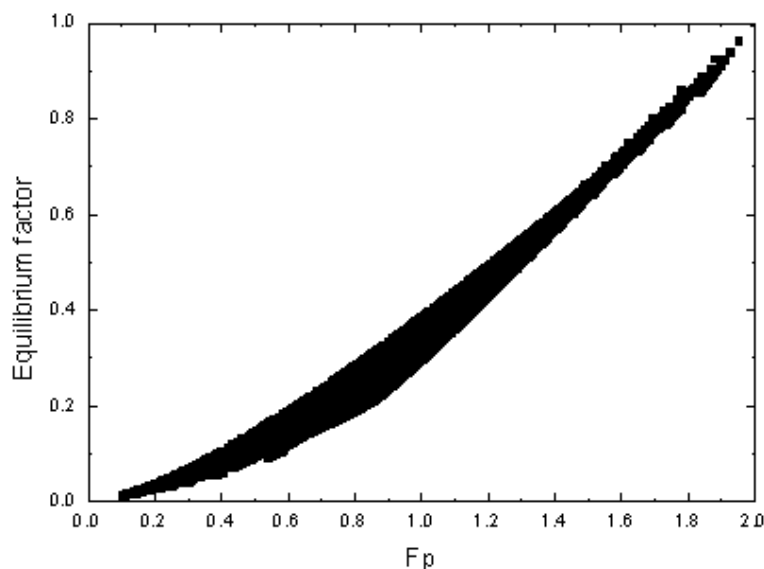
Figure 9. Dependence of the equilibrium factor F on the proxy equilibrium factor F_p ($= f_1 + f_3$) (adopted from Yu et al. (2005)).

4. FACTORS AFFECTING PARTIAL SENSITIVITIES OF BARE LR 115 DETECTOR

4.1. Removed Active Layer of the LR 115 Detector during Chemical Etching

As described in Eq. (4), the partial sensitivities can be determined from the track density ρ, the integrated radon exposure ($C_0 \times t$) and the proxy equilibrium factor F_p. After chemical etching and determination of the removed active layer thickness, the alpha-particle tracks registered by the LR 115 detector are counted under an optical microscope with 200× magnification. Only those tracks completely perforated the active layer of the LR 115 detector were counted. The track densities ρ (number of tracks per unit area) are then found. There have been two separate studies which determined the relationship between the partial sensitivity and removed active layer thickness of the LR 115 detector.

Leung et al. (2006) sent LR 115 detectors to the Health Protection Agency (HPA), Chilton, UK, for exposure in their walk-in exposure chamber with the volume of 43 m^3. The HPA staff adjusted the conditions inside the exposure chamber according to the requests and the detectors were then placed inside. To ensure that the F_p method was valid, there should not be surfaces or objects at distances shorter than R_{max} in front of the detectors. The highest alpha energy in the radon chain is 7.69 MeV (from ^{214}Po) and the corresponding range in air is 6.78 mm. The detectors were mounted onto a post placed at the centre of the exposure chamber, which was away from the walls much farther than 70 mm.

The reference value of the integrated radon exposure ($C_0 \times t$) and the equilibrium factor F inside the exposure chamber during the exposure period were provided by HPA as 100±5 kBqm^{-3}h and 0.680±0.068, respectively. After exposure, the detectors were returned back to

the laboratory for analyses. From the equilibrium factor of 0.680±0.068 provided by HPA, the corresponding F_p value was read from Figure 9. For the mid-point value of 0.680, F_p was determined to be from 1.51 to 1.57, and the mid value of this range (1.54) was used for subsequent calculations. The F interval from (0.680–0.068) to (0.680+0.068) then corresponded to an F_p interval from 1.37 to 1.67. Such an F_p interval was used in determining the relationship between the partial sensitivity and the removed active layer thickness as shown in Figure 10.

By fitting the linear relationship $\rho_i = A + Bx$ to the experimental data, where x (μm) was the removed active layer thickness of the LR 115 detector and ρ_i (m) was the partial sensitivity of the bare detector, Leung et al. (2006) obtained $A = -0.0041\pm0.0004$ and $B = 0.0011\pm0.0001$, with the coefficient of determination $R^2 = 0.9895$. The large value of R^2 showed that the variation in the partial sensitivity was well explained by the variation in the removed active layer thickness of the LR 115 detector. The fit was observed to be valid for the entire range of the present data set, in which the removed active layer thickness ranged from 5.3 to 6.6 μm.

Similarly, Yu et al. (2008) exposed LR 115 detectors to ^{222}Rn and its progeny inside an exposure chamber (Leung et al. 1994) filled with with radon gas generated from the 22.9 kBq radium (^{226}Ra) source. The reference value of the radon gas concentration was monitoried by a continuous radiation monitor. The aerosols were generated by an aerosol generator and injected regularly into the exposure chamber so as to maintain the equilibrium equivalent concentration (EEC) of the radon progeny concentration. The radon progeny concentration was measured by collecting them on a 47 mm diameter membrane filter. The alpha emissions from the collected progeny were read by a ZnS scintillator connected to a photomultiplier tube. Finally, the PAEC, EEC and the equilibrium factor of the progeny were calculated by the 3-count method.
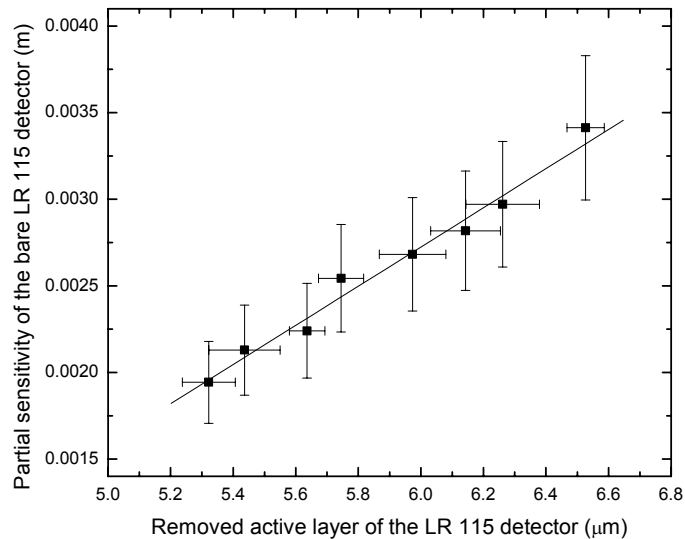

Figure 10. Relationship between the partial sensitivity ρ_i (m) of the bare LR 115 detector and the removed active layer thickness x (μm). The solid line is the best-fit line represented by $\rho_i = -0.0041 + 0.0011x$, with an R^2 of 0.9895. (Adopted from Leung et al. 2006.)

The experimental relationship between the partial sensitivity and the removed active layer thickness of the bare LR 115 detector obtained by Yu et al. (2008) is reproduced here in Figure 11. There were two sets of exposures. The radon gas concentration RC and the equilibrium factor F in sets 1 and 2 were found to be (1010±40 Bqm^{-3} and 0.148±0.022) and (1100±40 Bqm^{-3} and 0.109±0.012), respectively, with the uncertainties representing one standard deviations. The corresponding F_p value can be read from Figure 9. For the mid-point value of 0.148 and 0.109, F_p are determined to be from 0.47 to 0.71 with the mid-point 0.59, and from 0.38 to 0.60 with the mid-point 0.49, respectively. The F interval from (0.148–0.022) to (0.148+0.022) then corresponded to an F_p interval from 0.42 to 0.77, and the F interval from (0.109–0.012) to (0.109+0.012) to an F_p interval from 0.35 to 0.62. Such F_p intervals were used in determining the relationship between the partial sensitivity and the removed active layer thickness as shown in Figure 11.

By fitting the linear relationship $\rho_i = A + Bx$ to the present experimental data, where x (μm) is the removed active layer thickness of the LR 115 detector, Yu et al. (2008) obtained $A = -0.0055±0.0010$ and $B = 0.0015±0.0002$, with $R^2 = 0.9950$. The fit was valid within the entire range of the data set, which was from the removed active layer thickness 5.4 to 7.0 μm. It is interesting to note that the data collected from the two separate exposures closely follow the same trend.

It is remarked here that the linear relationships obtained by Leung et al. (2006) and Yu et al. (2008) agree very well with each other, within experimental uncertainties. It is also noted that the removed active layer thickness of the detector is a very critical parameter in determining the proxy-equilibrium factor F_p and hence F. Therefore, the removed layer thickness of the detector should be monitored carefully; otherwise errors will occur.
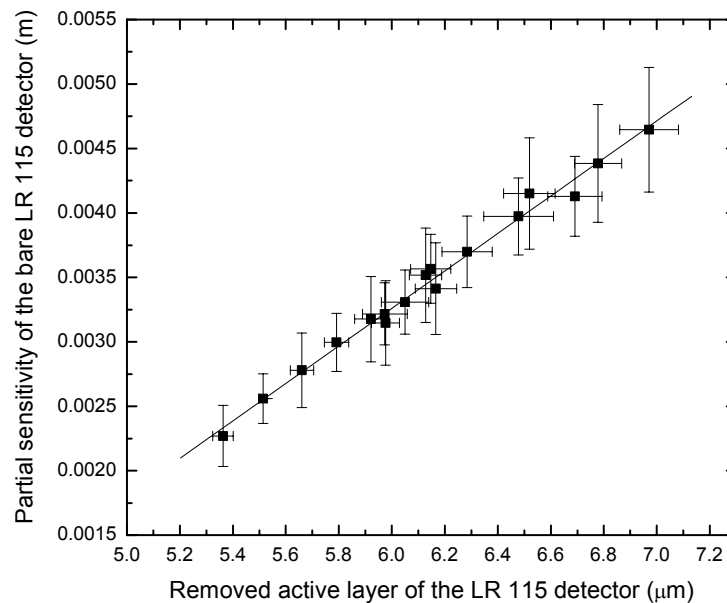

Figure 11. The relationship between the partial sensitivity ρ_i (m) of the bare LR 115 detector and the removed active layer thickness x (μm). The solid line is the best-fit line represented by $\rho_i = -0.00547 + 0.00145x$, with an R^2 of 0.9950. (Adopted from Yu et al. 2008.)

As noted at the beginning of section 3, the LR 115 detectors used were the Type 2 non-strippable detectors purchased from DOSIRAD, France. After the exposure process, the SSNTDs were etched in 10% aqueous NaOH at 60°C for approximately 1 h. The temperature was kept constant with an accuracy of ±1°C. The detectors were etched using a magnetic stirrer so as to provide faster etching (Yip et al., 2003a). After etching, the detectors were taken out of the etchant, rinsed with de-ionized water and dried.

As the partial sensitivities of the LR 115 detectors critically depend on the removed active layer thickness, measurements of the removed active layer thickness after chemical etching is required. Different methods have been used to measure the active layer thickness of LR 115 detectors, e.g., surface profilometry (Nikezic and Janicijevic, 2002; Yip et al., 2003a), absorption of x-ray fluorescence photons (Yip et al., 2003b), infrared absorption (Ng et al., 2004) and gray level determination (Yu and Ng, 2004). The infrared absorption method (Ng et al., 2004) is adopted in the work described here to measure the active layer thickness of LR 115 detectors. The active layer thickness of the detector was obtained through the infrared absorption determined using a Perkin-Elmer Fourier Transform Infrared (FTIR) spectroscopy system. The exponential decay relationship between the infrared transmittance at the wave number at 1598 cm^{-1} corresponding to the O–NO$_2$ bond and the thickness of the active layer (Ng et al., 2004) was used.

4.2. Presence of ^{220}Rn in the Ambient Environment

Thoron (^{220}Rn) and its progeny are also present in the ambient environment, which can affect the track densities on the bare LR 115 detector. Depending on the thoron gas concentration, thoron can contribute a significant amount of alpha tracks to the bare LR 115 detector. These extra alpha tracks will lead to erroneous estimate of F_p and hence F. In particular, enhancement of the track densities, ρ, on the bare LR 115 detector will overestimate F_p or even lead to out-of-range values (i.e., $F_p > 2$). Corrections should be performed to account for the number of tracks due to thoron on the bare detector.

To assess the possible effects of thoron, experimental calibration of the bare LR 115 detector to thoron inside the exposure chamber (Leung et al., 1994) was performed by Yu et al. (2008). Bare LR 115 detectors were placed inside the chamber with known thoron concentrations. After chemical etching and determination of the removed active layer thickness, the alpha particle tracks registered by the LR 115 detector were counted. Knowing the time of exposure and the thoron gas concentration, the partial sensitivities of bare LR 115 detector due to thoron corresponding to different removed active layer thickness were determined (Yu et al. 2008). The actual number of alpha-particle tracks due to a measured ^{220}Rn concentration can be subtracted in real life measurements.

The experimental relationship between the partial sensitivity to thoron of the bare LR 115 detector, γ, and the removed active layer thickness has been determined by Yu et al. (2008), which is reproduced here in Figure 12. By fitting the linear relationship $\gamma = A + Bx$ to the experimental data, where x (μm) is the removed active layer thickness of the LR 115 detector and γ (m) is the partial sensitivity to thoron of the bare LR 115 detector, Yu et al. (2008) obtained $A = -0.00887 \pm 0.00174$ and $B = 0.00319 \pm 0.00030$, with $R^2 = 0.9622$. The fit is

observed to be valid for the entire range of the present data set, in which the removed active layer thickness ranges from 5.3 to 6.5 μm.

The actual number of alpha tracks due to thoron, N_{Tn}, on the bare LR 115 detector can be calculated by:

$$N_{Tn} = c(Tn) \times t \times \gamma \times \text{(area of the bare LR 115 detector)} \qquad (6)$$

where $c(Tn)$ is the thoron gas concentration with the unit [Bqm^{-3}], t is the exposure time with the unit [s], γ is the partial sensitivity to thoron of the bare LR 115 detector with the unit [m].

4.3. Deposition of Dust Particles on the Bare LR 115 Detector

Yu et al. (2008) studied the possible effects of dust particles deposited on the surface of the bare LR 115 detector, and performed experiments to examine the track densities on (A) detectors placed in an indoor environment facing upwards so that dust particles could be deposited onto the detector, and (B) detectors same as (A) but cleaned with a brush everyday. The experiments were carried out at a site with a normal equilibrium factor (~0.35) and a site with a relatively high equilibrium factor (~0.6). The detectors were exposed for about 1 month and then sent back to laboratory for chemical etching and tracks analysis. The track densities can then be obtained for comparison.
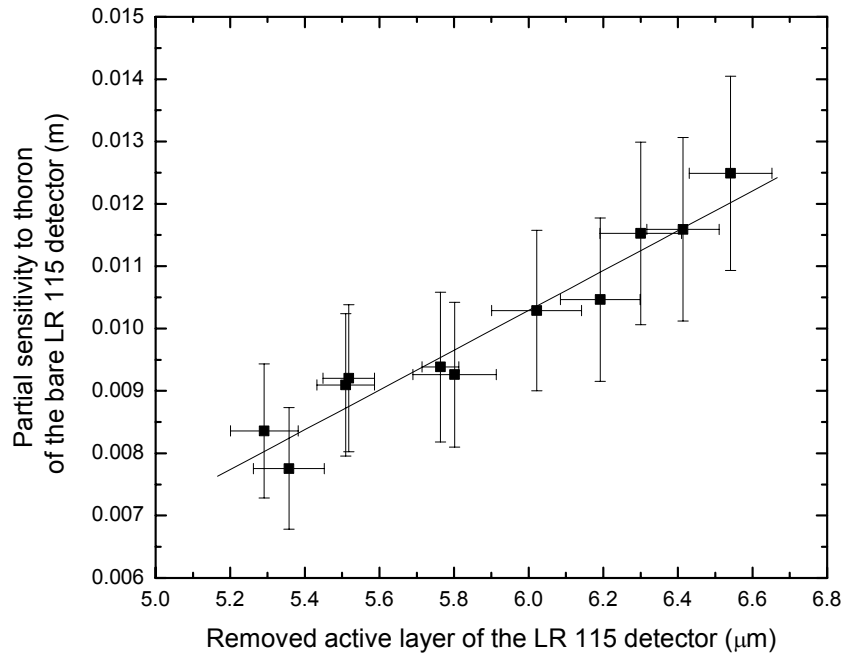

Figure 12. The relationship between the partial sensitivity to thoron γ (m) of the bare LR 115 detector and the removed active layer thickness x (μm). The solid line is the best-fit line represented by γ = −0.00887 + 0.00319x, with an R^2 of 0.9622. (Adopted from Yu et al. 2008.)

The numbers of alpha-particle tracks registered by the bare LR 115 SSNTD, the track densities and the measured removed active layer thickness are summarized in Table 2. In order to eliminate the effects from the variation of the removed active layer thickness of the detector, Yu et al. (2008) used a ratio R for this purpose, which was defined as:

$$R = (F_p + 1) \times (C_o \times t) = \frac{\rho}{\rho_i} \qquad (7)$$

In each exposure, F_p, C_0 and t, and thus also R were independent of the removed active layer thickness of the detector.

From Table 2, it can be seen that from exposures at both sites, the two detectors showed similar R values. Yu et al. (2008) thus concluded that the deposition of dust particles on the bare LR 115 detector would not contribute significant effects. Based on these experimental results, we can therefore ignore the deposition of dust particles on the bare LR 115 detector in determination of F. This finding is particularly important for the success of the F_p method because it will be otherwise too inconvenient to apply the method.

To understand why the deposition of dust particles on the bare LR 115 detector would not affect the track densities recorded on the LR 115 detector, Yu et al. (2008) also performed computer simulations on the partial sensitivities to the airborne ^{222}Rn, ^{218}Po and ^{214}Po for the LR 115 detector covered with a layer of SiO_2 with different thickness, for a nominal removed layer of 6 μm during the chemical etching of the exposed LR 115 detector. The SiO_2 layer was used to simulate the dust layer. The simulation results from Yu et al. (2008) are reproduced here in Figure 13. From Figure 13, we can see that even for the heavy SiO_2 layer, the partial sensitivities are equal to one another for a thickness of 2 to 3 μm. Therefore, unless the indoor environment is extremely dusty or consistently has heavy aerosols, the deposition of dust particles on the bare LR 115 detector will not affect the track densities recorded on the LR 115 detector.

Table 2. Comparisons of the number of tracks counted on the bare LR 115 SSNTDs and the corresponding track densities for (A) detectors facing upwards so dust particles can be deposited on the detector, and (B) detectors same as (A) but cleaned with a brush everyday. The removed active layers of the LR 115 SSNTDs are measured by FTIR and the ratios R are given for identification of effects of dust particles on the bare detector. (Adopted from Yu et al. 2008)

Exposure	Detector	Number of alpha tracks counted	Track density (10^5 m^{-2})	Removed active layer thickness (μm)	R (10^8 track/m^3)
1	A	560±40	5.95±0.42	6.05±0.14	1.81±0.19
	B	564±40	5.90±0.41	6.16±0.08	1.70±0.19
2	A	745±53	7.91±0.55	6.43±0.10	2.05±0.22
	B	759±54	8.07±0.56	6.52±0.11	2.03±0.22
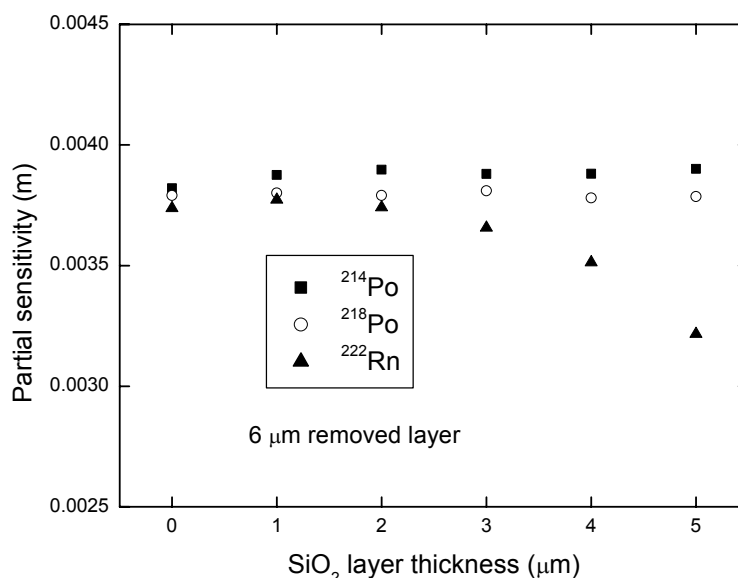
Figure 13. Computer simulation results on the partial sensitivities to the airborne ^{222}Rn, ^{218}Po and ^{214}Po for the LR 115 detector covered with a layer of SiO$_2$ with different thickness, for a nominal removed layer of 6 μm during the chemical etching of the exposed LR 115 detector. (Adopted from Yu et al. 2008.)

5. APPLICATIONS OF LONG-TERM RADON PROGENY CONCENTRATION MEASUREMENTS USING THE F_P METHOD

5.1. Long-Term Measurements of RC, TC and F in Dwellings

Yu et al. (2008) surveyed radon and thoron gas concentrations in 11 different indoor environments in different seasons, by making use of the "twins diffusion chamber" method (Virk and Sharma, 2000; Barooah et al., 2003; Sreenath Reddy et al., 2004; Leung et al. 2007b,c), and also F at the same time using the F_p method. At each site, two diffusion chambers were set-up; one covered with filter paper and the other with an optimal thickness of polyethylene membranes to measure the radon and thoron gas concentrations (Leung et al. 2007c). An LR 115 SSNTD with a size of 3×3 cm^2 was attached to the center of the inner bottom of each diffusion chamber. In addition, one bare mode LR 115 detector, also with a size of 3×3 cm^2, was attached on the outside of the top lid of the diffusion chambers to determine F_p.

Yu et al. (2008) performed two rounds measurements in the same dwellings but in different seasons. The periods were from mid-September to October, 2005 (summer/spring seasons) and February to mid-March, 2006 (winter/autumn seasons). After the desired exposure period, the diffusion chambers were collected from the dwellings and sent back to laboratory for chemical etching and tracks analysis. The radon and thoron gas concentrations and F could then be obtained.

The average F values for round 1 and 2 measurements were found as 0.47-0.56 and 0.52-0.60, respectively. Yu et al. (2008) attributed the slightly higher average equilibrium factor for round 2 measurements to the drier weather and thus the larger airborne aerosol concentrations in the winter/autumn seasons. The average F values for the two rounds of measurements lie in the range 0.49-0.58, with the mean equilibrium factor $F = 0.54$.

In order to estimate the effective dose from radon progeny, the methodology usually adopted in practice is to determine the radon gas concentration and to assume nominal F values, typically from 0.4 to 0.5. The need to assume nominal F values is unavoidable if no actual measurements of F can be made. However, due to the spatial and temporal fluctuations of environmental parameters, such as ventilation, aerosol concentrations, surface deposition, etc., the concentrations of radon and its progeny will vary, so an assumed constant F cannot reflect the actual conditions for many realistic situations. Yu et al. (2008) found large variations of F in dwellings, which ranged from 0.18 to 0.89. From the variations in the F values, there is no doubt that the use of an assumed constant F to calculate the effective dose does present a problem. Therefore, F should be measured at each site, and long-term measurements of F using F_p is suitable for this purpose. To obtain an even more accurate estimation of the effective dose, aerosol related parameters as well as subject related parameters are also needed.

5.2. Passive Monitoring of Equilibrium Factor inside a Radon Exposure Chamber

As mentioned in section 1, methods for long-term monitoring of the concentrations of radon progeny or F have been actively explored. The reliability of these methods invariably depends on the validity and accuracy of calibrations, for which exposure chambers are indispensable. While relatively small-size laboratory-based exposure chambers for ^{222}Rn gas are relatively easy to construct and operate (Yu et al., 2002), those for ^{222}Rn progeny are more complicated (e.g., Leung et al. 1994). In particular, the PAEC or F values inside the exposure chambers for ^{222}Rn progeny are usually monitored through active grab sampling, which can sometimes present problems since the aerosol concentrations (and thus the PAEC and F) can be significantly disturbed. In order to avoid excessive disturbance of the conditions inside the exposure chamber, the grab sampling cannot be carried out too frequently. Therefore, some changes in the PAEC inside the exposure chamber might not be adequately reflected by such short-term grab samplings. An alternative is to resort to a huge radon chamber, such as that of Health Protection Agency (HPA), UK, which has a volume of 43 m^3. In such a big chamber, the disturbance of the aerosol concentrations and thus the PAEC and F will be negligible during the active grab sampling. However, it would be more convenient and economical if the PAEC and F in laboratory-based exposure chambers for radon progeny can be correctly measured.

Leung et al. (2006) proposed to use the F_p method for passive monitoring of the equilibrium factor F inside a radon exposure chamber, which would not disturb the aerosol concentrations or the PAEC and which would give an integrated average value over the entire exposure period. This method might also be useful for exposure chambers for animals for epidemiological studies, for which the determination of radon progeny concentrations is also sometimes a challenge (Strong et al. 1996).

To verify the method, Leung et al. (2006) sent six LR 115 detectors to HPA for exposure in their walk-in exposure chamber. The LR 115 detectors (Type 2, non-strippable) used were purchased from DOSIRAD, France. The size of the detectors employed in the experiments was 3×3 cm^2. The reference value of the integrated radon exposure and the equilibrium factor inside the exposure chamber during the exposure period were provided by HPA as 100 ± 5 kBqm^{-3}h and 0.680 ± 0.068, respectively.

After exposure, the detectors were returned back to the laboratory for analyses. The LR 115 detectors were etched in 10% aqueous solution of NaOH maintained at 60°C by a water bath. The temperature was kept constant with an accuracy of $\pm1^o$C. During the etching process, the etchant was stirred continuously to provide more uniform etching. After etching for ~1 h, the detectors were removed from the etchant, rinsed with de-ionized water and dried. The removed active layer of the LR 115 detector was determined through the infrared transmittance at the wave number 1598 cm^{-1} (Leung et al. 2006).

From section 4.1, the relationship between the partial sensitivity ρ_i (m) and the removed active layer thickness x (μm) was shown to be $\rho_i = (-0.0041\pm0.0004) + (0.0011\pm0.0001)x$, which was employed to determine the partial sensitivities. The results are shown in Table 3. All the determined ranges of F overlapped with the experimental value of 0.680 ± 0.068. In particular, the mid points of the ranges fell between 0.578 to 0.768, with a mean of 0.69, so the mean of the mid points of the determined ranges of F for a few LR 115 SSNTDs could give a very good estimate of the true equilibrium factor (Leung et al. 2006).

5.3. Derivation of *V* Function for LR 115 SSNTDs

Effective use of SSNTDs relies on the understanding of development of alpha-particle tracks in these detectors, which has been suggested to base on two parameters, V_t and V_b, by Fleischer et al. (1975), where V_t is the track etch rate (i.e., the rate of etching along the particle trajectory) and V_b is the bulk etch rate (i.e., the rate of etching of the undamaged detector surface) or, equivalently, on the ratio $V = V_t/V_b$. Using the V function, together with a track growth model (e.g., Nikezic and Yu, 2003a), the alpha-particle track parameters including the lengths of the major and minor axes, can be calculated, and their profiles can be plotted (Nikezic and Yu, 2002b, 2003b, 2006).

Table 3. The removed layer, the partial sensitivities, the values of F_p and F determined for six LR 115 SSTNDs. The experimental value of F is 0.680 ± 0.068. (Adopted from Leung et al. 2006.)

Detector	Removed layer (μm)	Partial Sensitivity (m)	F_p	F
1	5.418±0.071	0.00206199	1.65	0.728–0.773
2	5.548±0.083	0.00220968	1.40	0.534–0.622
3	5.600±0.059	0.00226584	1.51	0.622–0.686
4	5.951±0.122	0.00266462	1.63	0.713–0.761
5	6.095±0.073	0.00282779	1.67	0.747–0.788
6	6.496±0.102	0.00328036	1.55	0.649–0.711

Most derivations of the V function for alpha-particle tracks in the LR 115 SSNTD relied on measurements of the dimensions of the alpha-particle tracks (e.g., Yip et al., 2006). Leung et al. (2007a) developed a method based on the sensitivity of the LR 115 SSNTD, i.e., the *number* of etched tracks completely penetrating the active cellulose nitrate layer. The method made use of F_p, and the experiments involved the determination of the sensitivities of the bare LR 115 SSNTD to ^{222}Rn and its short-lived progeny for different removed active layer thickness.

In fact, Leung et al. (2007a) made use of the data from exposing the bare LR 115 SSNTDs in the walk-in exposure chamber at HPA (Leung et al. 2006) as described in sections 4.1 and 5.2. The track growth model of Nikezic and Yu (2003a) was employed for calculations. Inputs into the model included the V function and the removed active layer during chemical etching. The incident energies of alpha particles from ^{222}Rn and its short-lived progeny on the LR 115 SSNTD were used to calculate their ranges in the detector material, which were accomplished using the SRIM program (http://www.srim.org/), with the LR 115 detector represented by cellulose nitrate (with the chemical composition $C_6H_8O_9N_2$ and a density $\rho = 1.4$ g cm^{-3}). The V function published by Durrani and Green (1984) was adopted in the their investigation in a modified form (referred to as the Durrani and Green function). The form of this function was:

$$V = \frac{V_t}{V_b} = 1 + (a_1 e^{-a_2 R} + a_3 e^{-a_4 R}) \cdot (1 - e^{-a_5 R}) \tag{8}$$

where R was the residual range of the alpha particles. The constants a_1, a_2, a_3, a_4 and a_5 for the function in Eq. (8) were given by Durrani and Green (1984) as 100, 0.446, 4, 0.044 and 1, respectively, and by Durrani and Bull (1987) as 100, 0.446, 5, 0.107 and 1, respectively.

The experimental data for ρ_i ($\rho_{i,\exp}$) were used to determine the new constants. Leung et al. (2007a) systematically adjusted the constants a_k, where $k = 1$ to 4, while keeping $a_5 = 1$, in order to obtaining the best agreement with their experimental data points through minimization of N defined as:

$$N = \sum_{j=1}^{14} \sqrt{[\rho_{i,\exp}(j) - \rho_{i,calc}(j)]^2} \tag{9}$$

where $\rho_{i,\exp}$ and $\rho_{i,calc}$ are the partial sensitivities obtained from experiment and simulation, respectively. The constant a_1 was changed from 5.0 to 25.0 with steps of 5.0; the constant a_2 from 0.2 to 0.6 with steps of 0.05; the constant a_3 from 4.0 to 7.0 with steps of 0.5 and the constant a_4 from 0.06 to 0.09 with steps of 0.005. When the constants a_k are varied, N showed some oscillatory behavior. When the first run with the ranges and steps given above was finished and the best combination (where N was smallest) was found, the second run was performed by varying the constants about the best values obtained in the first run, with much smaller steps. This procedure was repeated several times in order to find the combination of constants that gave the smallest N.
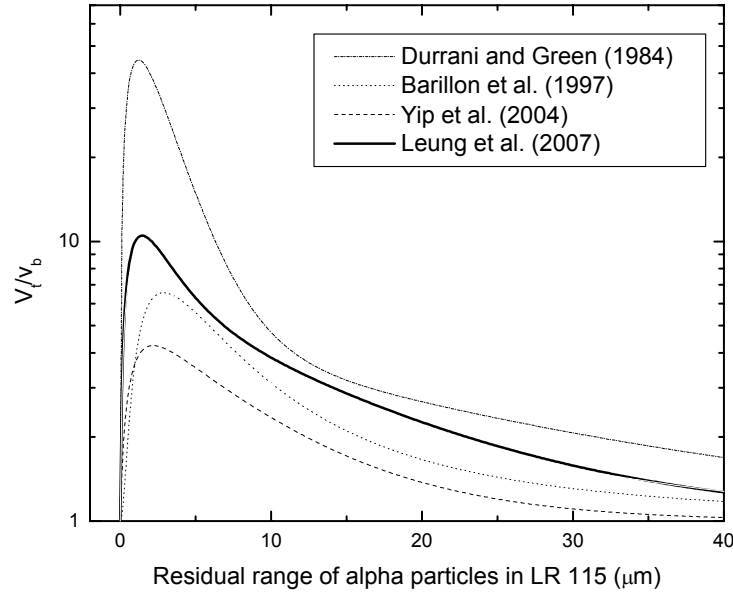
Figure 14. The V function ($=V_t/V_b$) derived from the partial sensitivity of the bare LR 115 detector obtained from experiments in the HPA exposure chamber. Also shown are three other previously derived V functions for comparison. (Adopted from Leung et al. 2007a.)

Three sets of simulations with the alpha energies 5.49, 6 and 7.69 MeV, which corresponded to ^{222}Rn, ^{218}Po and ^{214}Po, were performed. The final best estimated constants a_1, a_2, a_3 and a_4 were the average for these three sets of simulations. In this way, Leung et al. (2007a) found the best combination of constants as $a_1 = 14.23$; $a_2 = 0.48$; $a_3 = 5.9$ and $a_4 = 0.077$. Their V function was then obtained by substituting these constants into Eq. (8), which is shown in Figure 14.

The function from Durrani and Green (1984) given in Eq. (8) is also shown in Figure 14 for comparison. A maximum appears close to the end of the particle range, which corresponds to the Bragg peak in the stopping power curve. The maximum V_{max} was about 45, which might be too high since a nominal $V_b \approx 3.3$ μm h^{-1} (Nikezic and Janicijevic, 2002) would give $V_t \approx 150$ μm h^{-1} (Yip et al. 2006). Barillon et al. (1997) also published a V function for alpha-particle tracks in LR 115 in the form

$$V_t = V_b + \frac{1}{a_1^2 + \left[a_2 R - \dfrac{1}{a_3 R} \right]^2} \tag{10}$$

with constants $a_1 = 0.23$, $a_2 = 0.032$ and $a_3 = 3.8$, which is also shown in Figure 14.

Yip et al. (2006) also determined the V function for alpha-particle tracks in LR 115 in the form of the function of Durrani and Green (1984). They systematically irradiated LR 115 SSNTDs with alpha particles in the energy range from 1 to 5 MeV with incident angles from 30° to 90°. After chemical etching to remove a thickness of about 6.5 μm, the lengths of the

major and minor axes of the alpha-particle track openings in the films were measured with an image analyser. These data were used altogether to obtain the constants as $a_1 = 2.14$, $a_2 = 0.12$, $a_3 = 2.7$ and $a_4 = 0.135$ ($a_5 = 1$). This function is also shown in Figure 14 for a comparison.

From Figure 14, one can see that the function of Durrani and Green (1984) is very different from other three functions presented here, while these three functions are relatively commensurate among one another although there are some discrepancies. The discrepancies between the function derived by Yip et al. (2006) and those derived in the present work are worth particular mentioning, since the SSNTDs and the etching conditions have been the same in these two studies. The study of Leung et al. (2007a) was based on the track density while that of Yip et al. (2006) was based on the track opening dimensions. It seems that the results obtained from the track densities are different from those obtained using track-opening dimensions. The underlying reason is still unclear.

ACKNOWLEDGMENT

REFERENCES

Amgarou, K; Font, L; Baixeras, C. *Nucl Instrum Meth. A.*, 2003, *506*, 186-198.

Barillon, R; Fromm, M; Chambaudet, A; Marah, H; Sabir, A. *Radiat Meas.*, 1997, *28*, 619-628.

Barooah, D; Laskar, I; Goswami, AK; Ramachandran, TV; Nambi, KSV. *Radiat Meas.*, 2003, *36*, 461-463.

Dorschel, B; Piesch, E. *Radiat Prot Dosim.*, 1993, *48*, 145-151.

Durrani, SA; Bull, RK. *Solid state nuclear track detection. Principles, method and applications*. Pergamon Press, Oxford. 1987.

Durrani, SA; Green, PF. *Nucl Tracks.*, 1984, *8*, 21-24.

Fleischer, RL. *Health Phys.*, 1984, *47*, 263-270.

Fleischer, RL; Price, PB; Walker, RM. *Nuclear track in solids. Principles and applications*. University of California Press, Berkley, 1975.

Frank, AI; Benton, EV. *Nucl Track Det.*, 1977, *1*, 149-179.

Hadler, JC; Paulo, SR. *Radiat Protec Dosim.*, 1994, *51*, 283-296.

Jacobi, W. *Health Phys.*, 1972, *22*, 441-450.

Leung, JKC; Jia, D; Tso, MYW. *Nucl Instrum Meth A.*, 1994, *350*, 566-571.

Leung, SYY; Nikezic, D; Leung, JKC; Yu, KN. *Nucl Instrum Meth B.*, 2007c, *263*, 311-316.

Leung, SYY; Nikezic, D; Leung, JKC; Yu, KN. *Nucl Instrum Meth B.*, 2007b, *263*, 306-310.

Leung, SYY; Nikezic, D; Yu, KN. *J Environ Radioact*, 2007a, *92*, 55-61.

Leung, SYY; Nikezic, D; Yu, KN. *Nucl Instrum Meth A.*, 2006, *564*, 319-323.

Lubin, JH; Boice, JD Jr.; Samet, JM. *Radiat. Res.*, 1995, *144*, 329-341

Muirhead, CR. In Radon Measurements by Etched Track Detectors: Applications to Radiation Protection, *Earth Sciences and the Environment*, Editors, Durrani, S.A; R. Ilic. World Scientific, Singapore: 243-257, 1997.

Nakahara, N; Kudo, H; Akiba, F; Murakami, Y. *Nucl Instrum Meth.*, 1980, *171*, 171-179.

Ng, FMF; Yip, CWY; Ho, JPY; Nikezic, D; Yu, KN. *Radiat Meas.*, 2004, *38*, 1-3.

Nikezic, D., Yu, KN. *Radiat Meas.*, 2003b, *37*, 595-601.

Nikezic, D; Baixeras, C. *Radiat Meas.*, 1996, *26*, 203-213.

Nikezic, D; Janicijevic, A. *Appl Radiat Isotopes.*, 2002, *57*, 275-278.

Nikezic, D; Ng, FMF; Yu, KN. *Appl Radiat Isotopes.*, 2004, *61*, 1431-1435.

Nikezic, D; Yu, KN. *Comput Phys Commun.*, 2006, *174*, 160-165.

Nikezic, D; Yu, KN. *Mat Sci Eng R.*, 2004, *46*, 51-123

Nikezic, D; Yu, KN. *Nucl Instrum Meth A*, 1999, *437*, 531-537.

Nikezic, D; Yu, KN. *Nucl Instrum Meth B.*, 2002a, *187*, 492-498.

Nikezic, D; Yu, KN. *Nucl Instrum Meth B.*, 2002b, *196*, 105-112.

Nikezic, D; Yu, KN. *Radiat Meas.*, 2003a. *37*, 39-45.

Nikolaev, V. A; Ilic, R. *Radiat Meas.*, 1999, *30*, 1-13.

NRC (National Research Council), *Health effects of exposure to radon*. National Academic Press, Washington, D.C. 1999

Planinic, J; Faj, Z. *Health Phys.*, 1990, *59*, 349-351.

Reddy, MS; Reddy, PY; Reddy, KR; Eappen, KP; Ramachandran, TV; Mayya, YS. *J Environ Radioactiv.*, 2004, *73*, 21-28.

Somogyi, G; Hunyadi, I; Varga, Z. *Nucl Track Det.*, 1978, *2*, 191-197.

Strong, JC; Morlier, JP; Monchaux, G; Bartstra, RW; Groen, JS; Baker, ST. *Appl Radiat Isotopes.*, 1996, *47*, 355-359.

Virk, HS; Sharma, N. *Appl Radiat Isotopes*, 2000, *52*, 137-141.

Yip, CWY; Ho, JPY; Koo, VSY; Nikezic, D; Yu, KN. *Radiat Meas.*, 2003a, *37*, 197-200.

Yip, CWY; Ho, JPY; Nikezic, D; Yu, KN. *Radiat Meas.*, 2003b, *36*, 161-164.

Yip, CWY; Nikezic, D; Ho, JPY; Yu, KN. *Mater Chem Phys.*, 2006, *95*, 307–312.

Yu, KN; Leung, SYY; Nikezic, D; Leung, JKC. *Radiat Meas.*, 2008, *43* (Suppl. 1), S357-S363.

Yu, KN; Ng, FMF. *Nucl Instrum Meth B.*, 2004, *226*, 365-368.

Yu, KN; Nikezic, D; Ng, FMF; Leung, JKC. *Radiat Meas.*, 2005, *40*, 560-568.

Yu, KN; Koo, VSY; Guan, ZJ. *Nucl Instrum Meth A*, 2002, *481*, 749-755.